Qiu *et al. BMC Cancer* (2025) 25:813
https://doi.org/10.1186/s12885-025-14212-x

BMC Cancer

RESEARCH Open Access

Single-cell sequencing unveils the transcriptomic landscape of castration-resistant prostate cancer-associated fibroblasts and their association with prognosis and immunotherapy response

Yifeng Qiu[1,2,3,6], Yuhan Wang[1,2,3], Jiahe Liu[1,2,3], Kai Sun[4,5], Baohua Liu[3*] and Qi Hou[2,3,6*]

Abstract

Background The tumor microenvironment (TME) is increasingly acknowledged as a determinant in the malignant transformation and progression of castration-resistant prostate cancer (CRPC). Cancer-associated fibroblasts (CAFs), as a pivotal stromal cellular component in TME, are implicated in tumor progression and immune escape. However, the molecular characteristics and biological functions of CRPC-CAFs in prostate cancer necessitate further investigation.

Methods We ascertained the differential transcriptomic profiles between CRPC-CAFs and PCa-CAFs through single-cell RNA-sequencing (scRNA-seq). Bulk RNA-seq data were employed to assess the prognostic implications of CRPC-CAFs in PCa. In addition, we examined the impact of CRPC-CAFs on the efficacy of immunotherapy and the composition of the tumor immune milieu. Furthermore, a subcutaneous PCa model was applied to determine the potential of TGF-β signaling blockade to augment the response to immunotherapeutic interventions.

Results We observed a pronounced increase in the proportion of CAFs in CRPC compared to those in primary PCa. The functional pathways implicated in TGF-β signaling and ECM remodeling were remarkably upregulated in CRPC-CAFs. Moreover, gene regulatory network analysis uncovered substantial differences in the transcription factor activity profiles between CRPC-CAFs and PCa-CAFs. The elevated CRPC-CAFs abundance was associated with diminished recurrence-free survival and immunotherapy insensitivity. Substantially elevated infiltration of inhibitory immune cells and upregulated expression levels of immunosuppressive molecules were observed in patients with high CRPC-CAFs abundance. Importantly, administration of anti-TGF-β therapy remarkably potentiated the efficacy of anti-PD-1 immunotherapy through upregulating the anti-tumor immune response in the PCa model.

Conclusion Our results highlighted the impact of CRPC-CAFs on clinical prognosis and immunosuppressive tumor milieu, indicating that CRPC-CAFs may function as a promising therapeutic target for CRPC.

*Correspondence:
Baohua Liu
ppliew@szu.edu.cn
Qi Hou
qi_hou@foxmail.com

Full list of author information is available at the end of the article

Keywords Castration-resistant prostate cancer, Cancer-associated fibroblasts, Single-cell RNA-sequencing, Clinical outcomes, Immune infiltration

Background

Based on the latest global cancer statistics, prostate cancer (PCa) is the second most frequently diagnosed malignancy among men, with an estimated 1.47 million new cases and 396,792 deaths globally in 2022 [1]. Androgen deprivation therapy (ADT) is the standard and effective treatment for advanced PCa and biochemical recurrence following active local therapy [2, 3]. Nevertheless, a substantial number of PCa patients develop resistance to ADT within 2–3 years, leading to disease progression to castrate-resistant prostate cancer (CRPC) [4]. Despite significant advancements in therapeutic modalities, including next-generation androgen receptor antagonists, chemotherapeutic agents, and poly (ADP-ribose) polymerase (PARP) inhibitors, patients with CRPC frequently encounter unfavorable clinical outcomes [5, 6]. Therefore, a comprehensive understanding of the molecular mechanisms underlying CRPC is crucial for developing new strategies to prevent ADT resistance and improve prognosis.

Previously, CRPC was primarily attributed to the dysregulation of androgen receptor (AR) signaling pathways within tumor cells, including increased expression of AR splice variants, mutations, and genomic rearrangements [7, 8]. Recently, a burgeoning body of evidence has underscored the pivotal role of the tumor microenvironment (TME) remodeling in development and progression of CRPC [9–11]. Cancer-associated fibroblasts (CAFs) represent a paramount stromal cell subset within the TME. Previous studies have demonstrated that CAFs play an indispensable role in cancer progression, dissemination, and creation of an immunosuppressive TME [12–14]. In the context of PCa, CAFs have been reported to confer chemoresistance to cancer cells, mediated by upregulation of glutathione synthesis and reduction in the production of reactive oxygen species (ROS) [15]. It has been demonstrated that chemotherapy elicits the release of WNT16B from CAFs, consequently attenuating the sensitivity of cancer cells to chemotherapeutic agents and accelerating the progression of PCa [16]. CAFs are also recognized as critical modulators in the progression of CRPC and neuroendocrine differentiation. For instance, neuregulin1 (NRG1), a ligand secreted by CAFs, has been found to compromise the efficacy of ADT through the activation of HER3 signaling. Elevated levels of NRG1 activity in patients correlate with an unfavorable prognosis [17]. Following castration treatment, CAFs exhibit diminished expression of SPARC and enhanced secretion of IL-6, which potentially fosters neuroendocrine differentiation in CRPC [18]. Moreover, CAFs are reported to facilitate the expression of 3β-Hydroxysteroid dehydrogenase-1 (3βHSD1) in cancer cells through paracrine signaling mechanisms involving glucosamine, eventually contributing to ADT resistance [19]. Recent advances in scRNA-seq have provided insights into the phenotypic and functional diversity of distinct stromal and immune cells in PCa [20, 21]. However, the molecular and biological characteristics of castration-resistant prostate cancer-associated fibroblasts (CRPC-CAFs) and their impact on prognosis and immune TME in PCa remain to be fully elucidated.

In this research, we conducted a comprehensive scRNA-seq analysis to delineate the dynamic alterations in biological functions between PCa-CAFs and CRPC-CAFs. Notably, CRPC-CAFs were characterized by remarkable upregulation of TGF-β signaling. Patients with higher CRPC-CAFs abundance exhibited unfavorable clinical outcomes in PCa and diminished responsiveness to immunotherapy. Furthermore, through a subcutaneous tumor-bearing mouse model, we demonstrated that targeted inhibition of TGF-β signaling could augment the anti-PD-1 immunotherapy response and restrain tumor growth in vivo. Collectively, these results indicate that the combination of TGF-β signaling inhibition and immunotherapy represents a promising therapeutic strategy to improve clinical outcomes for patients with CRPC.

Methods

Data collection

The single-cell RNA-seq datasets GSE141445 (comprising 13 primary PCa samples) and GSE210358 (comprising 13 CRPC samples) were retrieved from the Gene Expression Omnibus (GEO) database (http://www.ncbi.nlm.nih.gov/) [20, 22]. Bulk RNA-seq data from the TCGA-PRAD cohort were obtained from the UCSC Xena website (https://xenabrowser.net/). Microarray data from the GSE70769 and GSE21034 PCa cohorts were downloaded from the GEO database. Bulk RNA-seq data from the IMvigor210 immunotherapy cohort were accessed by utilizing the "IMvigor210CoreBiologies" R package. In addition, microarray data from the GSE32269 and GSE70768 datasets were acquired to compare CRPC-CAFs signature scores between primary PCa and metastatic CRPC tissues.

Single-cell RNA-seq data processing and cell-type annotation

R software (version 4.2.0) and the "Seurat" package (version 4.1.1) were utilized to process and analyze the

scRNA-seq data. For filtering, cells with a mitochondrial gene proportion exceeding 10% or with an expressed gene count below 200 or above 5000 were excluded. Subsequently, the scRNA-seq data were normalized, and batch effects across different samples were corrected by using the "Harmony" method [23]. Principal component analysis (PCA) was conducted on the expression of the top 2000 highly variable genes, and the top 30 principal components were used for clustering analysis at a resolution of 0.5. The following canonical markers were employed to perform manual cell-type annotation: Epithelial cells (EPCAM, KRT19), Fibroblasts (DCN, COL1A1), Smooth muscle cells (MYH11, ACTA2, RGS5), Endothelial cells (VWF, PECAM1, CLDN5), T cells (CD2, CD3D, CD3E), B cells (CD79A, CD79B, CD19), Masts (TPSB2, TPSAB1, MS4A2), Myeloid cells (CD14, CD68, AIF1, CSF1R) [20, 22, 24–26].

Differential expression analysis

Differential expression analysis was conducted using FindAllMarkers function (with parameters set to min.pct = 0.25 and only.pos = TRUE) in "Seurat" package. Genes with avg_log2FC ≥ 1 and adjust p-value < 0.05 were identified as marker genes in PCa-CAFs and CRPC-CAFs subgroups.

Pathway enrichment analysis

We performed Gene Ontology (GO) enrichment analysis on marker genes of CRPC-CAFs by utilizing "ClusterProfiler" package [27]. Subsequently, Gene Set Enrichment Analysis (GSEA) was employed to further determine the markedly upregulated or downregulated signaling pathways in CRPC-CAFs, using gene sets from the Molecular Signature Database [28]. Furthermore, the AUCell analysis was conducted to evaluate the activity levels of various signaling pathways.

Gene regulatory network analysis

We applied pySCENIC (version 0.12.0) to assess the activity of transcription factor (TFs) in PCa-CAFs and CRPC-CAFs subgroups [29]. The GRNBoost algorithm was employed to establish co-expression networks for TFs and their target genes. Subsequently, we conducted *cis*-regulatory motif analysis and identified regulons by utilizing RcisTarget method. Additionally, the AUCell algorithm was employed to quantify the activity scores of regulons.

Single-cell trajectory analysis and cell–cell communication analysis

The Monocle (version 2.24) algorithm was utilized to develop pseudo-time trajectories of CAFs and decipher the dynamics of gene expression changes in CAFs during the progression from primary PCa to CRPC [30]. CellChat (version 1.6.1) was applied to conduct a comprehensive analysis of intercellular communication between CAFs and other cell types in PCa and CRPC, using the CellChatDB.human reference database [31].

Definition and the prognostic significance of CRPC-CAFs signature scores

A set of marker genes of CRPC-CAFs were used to construct a novel signature. The CRPC-CAFs signature scores for TCGA, IMvigor210 and GEO cohorts were computed using the "ssGSEA" algorithm. Kaplan-Meier analysis and the log-rank test were conducted to assess the difference in recurrence-free survival between patients with high versus low CRPC-CAFs signature scores.

Tumor microenvironment analysis

Stromal and immune scores were computed through ESTIMATE analysis [32]. Additionally, we employed CIBERSORT and ssGSEA to assess the infiltration of various immune cell types [33, 34]. Furthermore, the xCell algorithm was utilized to quantify the density of 64 stromal and immune cell types [35].

Immunotherapy response prediction

The Tumor Immune Dysfunction and Exclusion (TIDE) score was employed to assess immune evasion status and predict efficacy of immunotherapy in cancer patients [36]. An elevated TIDE score is indicative of poorer response to immunotherapy.

Cell culture and treatment

The RM-1 murine prostate cancer cell line and the WPMY-1 human immortalized prostatic fibroblast cell line, both acquired from Pricella Biotechnology Co., Ltd. (Wuhan, China), were cultivated in DMEM (Gibco) supplemented with 10% FBS and 1% penicillin-streptomycin solution under a 5% CO_2 atmosphere at 37 °C. The recombinant human TGF-β1 protein was purchased from MedChemExpress.

Animal models

Eight-week-old male C57BL/6J mice were procured from Weitong Lihua Experiment Animal Technology Co., Ltd. (Beijing, China). All animal procedures were sanctioned by the Institutional Animal Care and Use Committee of Shenzhen University Medical School. RM-1 PCa cells (1×10^6) were subcutaneously implanted into the dorsal region of the mice. Upon reaching a tumor volume of approximately 100 mm^3, the tumor-bearing mice were randomly assigned to four distinct treatment groups. In the monotherapy group, either anti-PD-1 (10 mg/kg, #BE0146, BioXcell) or anti-TGF-β (10 mg/kg, #BE0057, BioXcell) was administered intraperitoneally every three

days. In the combination therapy group, both anti-PD-1 (10 mg/kg) and anti-TGF-β (10 mg/kg) were administered intraperitoneally every three days. The control group received an equivalent volume of isotype IgG intraperitoneally. Tumor volume was determined by using the formula: volume = (tumor length) × (tumor width)^2/2. At the end of the experiment protocol, mice were subjected to euthanasia in accordance with the American Veterinary Medical Association (AVMA) Guidelines for the Euthanasia of Animals (2020 Edition), and tumor samples were harvested for further analysis (Supplementary File 2).

Immunohistochemistry (IHC) staining

PCa tumor tissues were fixed by utilizing a 4% solution of paraformaldehyde and embedded in paraffin. Subsequently, antigen retrieval was executed and endogenous peroxidase activity was inhibited by using a 3% hydrogen peroxide solution. After blocking nonspecific antibody binding, the sections were incubated with primary antibodies overnight at 4 °C in a humidity chamber. The following primary antibodies were utilized in this study: CD4 (1:3000, ab183685, abcam), CD8 (1:2000, ab209775, abcam), TGF-β1 (1:2000, 21898-1-AP, Proteintech), α-SMA (1:2000, 19245 S, CST), PD-1 (1:500, ab214421, abcam), PD-L1 (1:50, 64988 S, CST). After the application of the secondary antibody, protein expression was detected by utilizing the chromogenic substrate 3,3'-diaminobenzidine (DAB). For each section, five discrete fields were randomly selected, and the number of CD4-positive or CD8-positive stained cells was quantified. The mean number of positive cells across these fields was calculated. The expression levels of TGF-β1, α-SMA, PD-1, and PD-L1 were assessed by calculating the percentage area (%Area) of positive staining in IHC images, as quantified by ImageJ software.

RNA extraction and transcriptome sequencing

The WPMY-1 cell line was subjected to treatment with recombinant TGF-β1 protein at a concentration of 10 ng/ml, with the phosphate-buffered saline (PBS) treatment functioning as the control. Total RNA was extracted from WPMY-1 cells using TRIzol reagent (Invitrogen), and the TruSeq RNA Library Prep Kit (Illumina) was employed to construct the RNA-Seq libraries. The Illumina Novaseq platform was applied to conduct RNA sequencing, yielding paired-end reads with a length of 150 bp. Subsequently, we utilized Hisat2 software for the alignment of sequencing reads to the human reference genome (GRCh38). The "edgeR" package was employed to conduct differential expression analysis between WPMY-1 cells treated with TGF-β1 and those in the control group. DEGs were discerned according to the following criteria:|log2 fold change| exceeding 1.5 and a false discovery rate (FDR) below the threshold of 0.05. We leveraged "ClusterProfiler" to conduct GSEA and subsequently utilized the "GseaVis" package for the visualization of the results. The "GSVA" package was applied to execute ssGSEA.

Quantitative real-time PCR (RT-qPCR)

Following the extraction of total RNA, reverse transcription was performed with PrimeScript RT Master Mix (Takara, Otsu, Shiga, Japan) to synthesize cDNA. RT-qPCR was achieved on QuantStudio 6 Real-Time PCR System (Applied Biosystems) by using SYBR Green mix (Takara). The primers used in this study were shown in Supplementary Table 1. The relative expression levels of genes were determined by using the $2^{-\Delta\Delta Ct}$ method. GAPDH was utilized to normalize the expression levels of the genes.

Cell proliferation analysis

The proliferative capacity of prostatic fibroblasts was assessed by utilizing the Cell Counting Kit-8 (MedChemExpress). WPMY-1 cells (5×10^3 cells) were seeded into 96-well plates and incubated for 24 h prior to treatment. Then, the cells were treated with either 0 or 10 ng/ml TGF-β1 protein. Following incubation for 0 h, 24 h, 48 h, and 72 h, a 10% solution of CCK-8 reagent was added to each well, and the cells were incubated at 37 ℃ for 2 h. The absorbance at 450 nm was measured.

Wound healing assay

WPMY-1 cells were plated into 6-well plates. Upon reaching a cell confluence of approximately 90%, linear wounds were created by utilizing a 200-μL sterile pipette tip. After removing cellular debris through PBS washing, the cells were incubated in serum-free medium supplemented with either 0 or 10 ng/ml of TGF-β1 protein. The wound closure was documented by utilizing a ZEISS microscope at 100× magnification. The areas of scratch healing were quantified using ImageJ software.

Western blot analysis

WPMY-1 cells were lysed using RIPA buffer to extract total cellular protein. SDS/PAGE gel electrophoresis was utilized to separate the proteins, which subsequently were transferred to PVDF membranes (Millipore, Billerica, MA, USA). Blocking of the membranes was achieved by utilizing a 5% no-fat milk solution, followed by incubation with specific primary antibodies at 4 °C overnight. Then, HRP-conjugated secondary antibodies were utilized to incubate the membranes, and ECL detection kit (ThermoFisher Scientific, Waltham, MA, USA) was employed to visualize the immunoblots. The primary antibodies utilized in this study are detailed as follows:

BGN (#16409-1-AP, Proteintech) and GAPDH (#60004-1-Ig, Proteintech).

Statistical analysis

All statistical analyses and data visualizations were conducted using R software (version 4.2.0) and GraphPad Prism (version 8.3.0). The correlation between two distinct continuous variables was assessed using Spearman's rank correlation analysis. For comparing continuous variables between two groups, we employed either a parametric t-test or a nonparametric Wilcoxon test, depending on the data distribution. In this study, statistical significance was set at a p-value threshold of 0.05.

Results

Single-cell sequencing revealed an increased proportion of CAFs in CRPC, and CRPC-CAFs were correlated with unfavorable prognosis

Following preprocessing and filtering, a total of 71,560 cells were selected and subjected to further analysis, comprising 36,424 cells from primary PCa and 35,136 cells from CRPC. Principal component analysis (PCA) was employed to achieve data dimensionality reduction, and we obtained 33 different clusters (Supplementary Fig. 1A). Eight major cell types were annotated according to their distinct expression patterns of canonical marker genes (Fig. 1A-B). CAFs were specifically identified through notably elevated expression levels of DCN and COL1A1 (Fig. 1C-D). To precisely distinguish between epithelial cells and CAFs, we undertook a comparative analysis of the canonical epithelial markers. The dot plot showed that the expression of KRT8, KRT18, AR, and KLK3 was either absent or markedly diminished in the CAFs population compared to epithelial cells, confirming that the DCN/COL1A1-positive population is comprised of CAFs rather than epithelial cells (Supplementary Fig. 1B). Importantly, a substantially elevated proportion of CAFs was observed in CRPC compared to primary PCa, indicating a critical role of CAFs in the progression to CRPC (Fig. 1E-F). Subsequently, a total of 2,641 CAFs were identified and classified into CRPC-CAFs and PCa-CAFs subgroups (Fig. 1G). Differential expression analysis was conducted, and we detected 62 marker genes significantly upregulated in CRPC-CAFs, including POSTN, COL1A1, COL1A2, FN1, COL3A1. In contrast, 69 marker genes were significantly upregulated in PCa-CAFs (Fig. 1H; Supplementary Table 2). To assess the abundance of CRPC-CAFs in PCa tissues, we employed ssGSEA to compute the CRPC-CAFs scores based on CRPC-CAFs marker genes. Notably, we observed significantly increased CRPC-CAFs scores in metastatic CRPC compared to localized PCa tissues in two distinct datasets (GSE32269 and GSE70768) (Supplementary Fig. 1C-D). To explore the prognostic significance of CRPC-CAFs, we conducted Kaplan-Meier analysis and found that patients with higher CRPC-CAFs scores had a more unfavorable recurrence-free survival than those with lower CRPC-CAFs scores in the TCGA, GSE70769, and GSE21034 cohorts (Fig. 1I-K). In summary, these data demonstrated that CRPC-CAFs were intricately associated with progression to CRPC and unfavorable prognosis of patients with PCa. It is essential to elucidate the functional characteristics of CRPC-CAFs.

CRPC-CAFs exhibited distinct functional characteristics compared to those of PCa-CAFs

To elucidate the biological functions of CRPC-CAFs, we conducted KEGG and GO enrichment analyses based on upregulated marker genes of CRPC-CAFs. KEGG analysis results showed that CRPC-CAFs were mainly implicated in focal adhesion, proteoglycans in cancer, and ECM-receptor interaction (Fig. 2A). GO enrichment analysis demonstrated that CRPC-CAFs were mainly involved in the processes of extracellular matrix remodeling and collagen organization (Fig. 2B). Additionally, GSEA results suggested that extracellular matrix remodeling-related signaling pathways were remarkably activated in CRPC-CAFs, whereas androgen response was downregulated in CRPC-CAFs (Fig. 2C-F). To discern the key genes contributing to these biological pathways, we conducted leading edge analysis and revealed the core enriched genes involved in the ECM remodeling process, including COL1A1, COL1A2, FN1, COL3A1, and TIMP1 (Supplementary Fig. 2A-C). These results suggested that the notable upregulation of these genes in CRPC-CAFs may play a paramount role in reshaping the tumor microenvironment in CRPC. A specific set of genes, such as KLK3, KLK2, FKBP5, STEAP4, and TSC22D1, are predominantly responsible for the suppression of the androgen response pathway (Supplementary Fig. 2D). The downregulated expression of these genes indicates a reduced sensitivity to androgen signaling in CRPC-CAFs, which is consistent with the development of castration resistance. Furthermore, AUCell analysis results indicated that the TGF-β signaling pathway was significantly activated in CRPC-CAFs compared with PCa-CAFs (Fig. 2G-H). Collectively, these findings demonstrated that CRPC-CAFs displayed a notable upregulation in TGF-β signaling and extracellular matrix remodeling.

Pseudotime trajectory analysis delineated the transcriptional transition from PCa-CAFs to CRPC-CAFs

To investigate the dynamic alteration between PCa-CAFs and CRPC-CAFs, we employed pseudotime analysis to construct the developmental trajectory of CAFs. The results demonstrated that PCa-CAFs were mainly located at the beginning of the developmental trajectory. As pseudotime increased, there was a progressive increase in

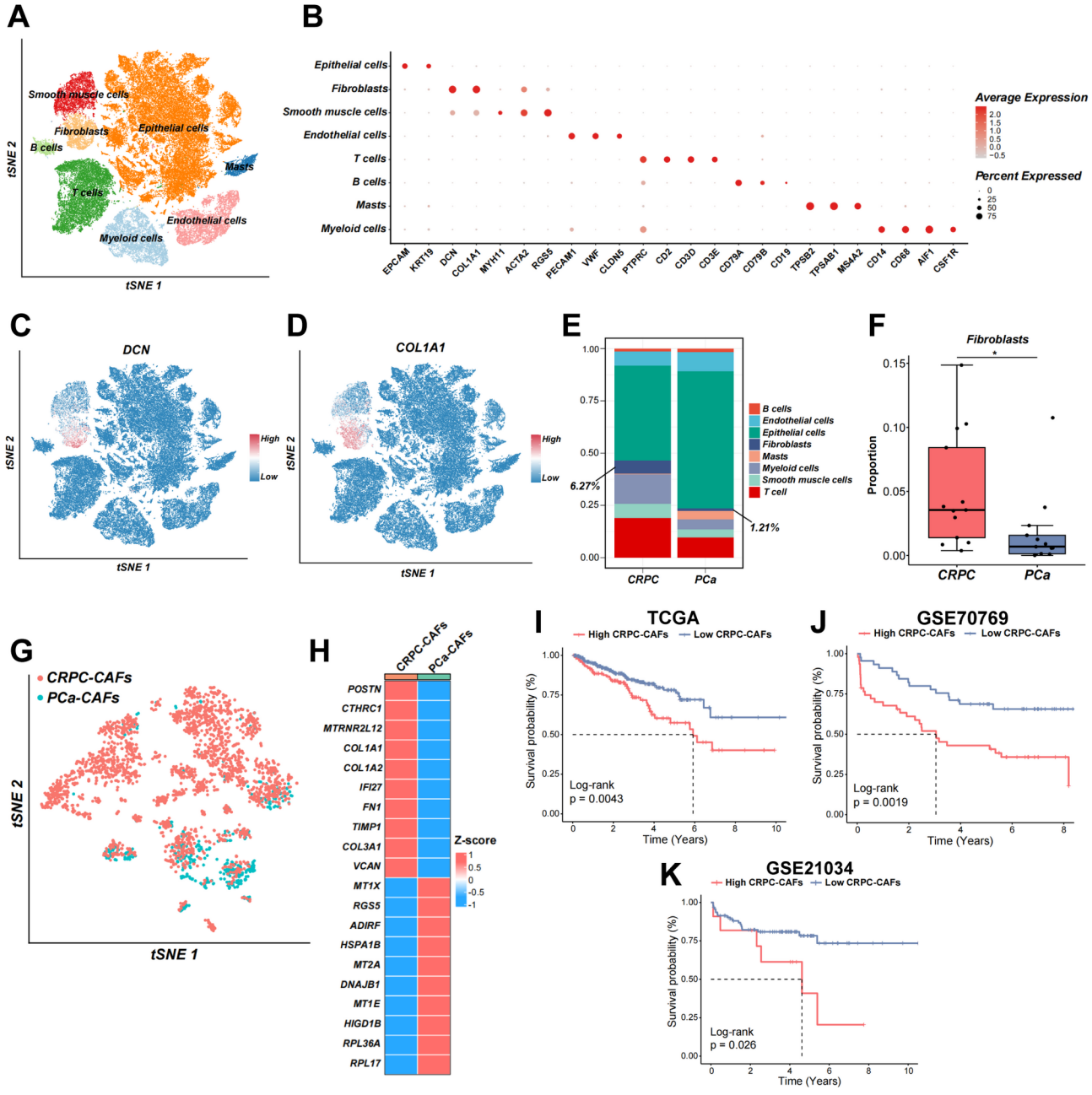

Fig. 1 Integrated scRNA-seq and bulk RNA-seq analyses dissecting the proportion and clinical significance of CRPC-CAFs. (**A**) t-SNE plot of 71,560 single cells derived from 13 primary PCa and 13 CRPC samples color-coded based on the main cell type. (**B**) Dot plot illustrating average expression level of marker genes across distinct cell types. (**C-D**) t-SNE plot displaying the expression levels of DCN and COL1A1. (**E**) Stacked bar plot presenting the proportions of eight distinct cell types in PCa and CRPC tissues. (**F**) Boxplot comparing the proportion of cancer-associated fibroblasts (CAFs) between PCa and CRPC tissues. Statistical significance was assessed using a two-tailed Wilcoxon test (*$p < 0.05$). (**G**) t-SNE plot displaying 2641 CAFs derived from PCa and CRPC samples. (**H**) Heatmap illustrating scaled average expression of top 10 marker genes in PCa-CAFs and CRPC-CAFs. (**I-K**) Kaplan–Meier curves presenting a comparison of recurrence-free survival between patients with high versus low CRPC-CAFs scores in the TCGA (**I**), GSE70769 (**J**) and GSE21034 (**K**) cohorts

the population of CRPC-CAFs, indicating a phenotypic transformation from PCa-CAFs to CRPC-CAFs state (Fig. 3A-C). Furthermore, our pseudotime trajectory analysis discerned a pronounced upregulation of genes in CRPC-CAFs that are implicated in ECM remodeling and tumor progression, including COL1A1, COL1A2, COL3A1, FN1, POSTN, and TIMP1 (Fig. 3D-E). In contrast, RGS5, ADIRF, DNAJB1, and HSPA1B were highly expressed at the early stage of the trajectory and then gradually decreased with pseudotime (Fig. 3E). The

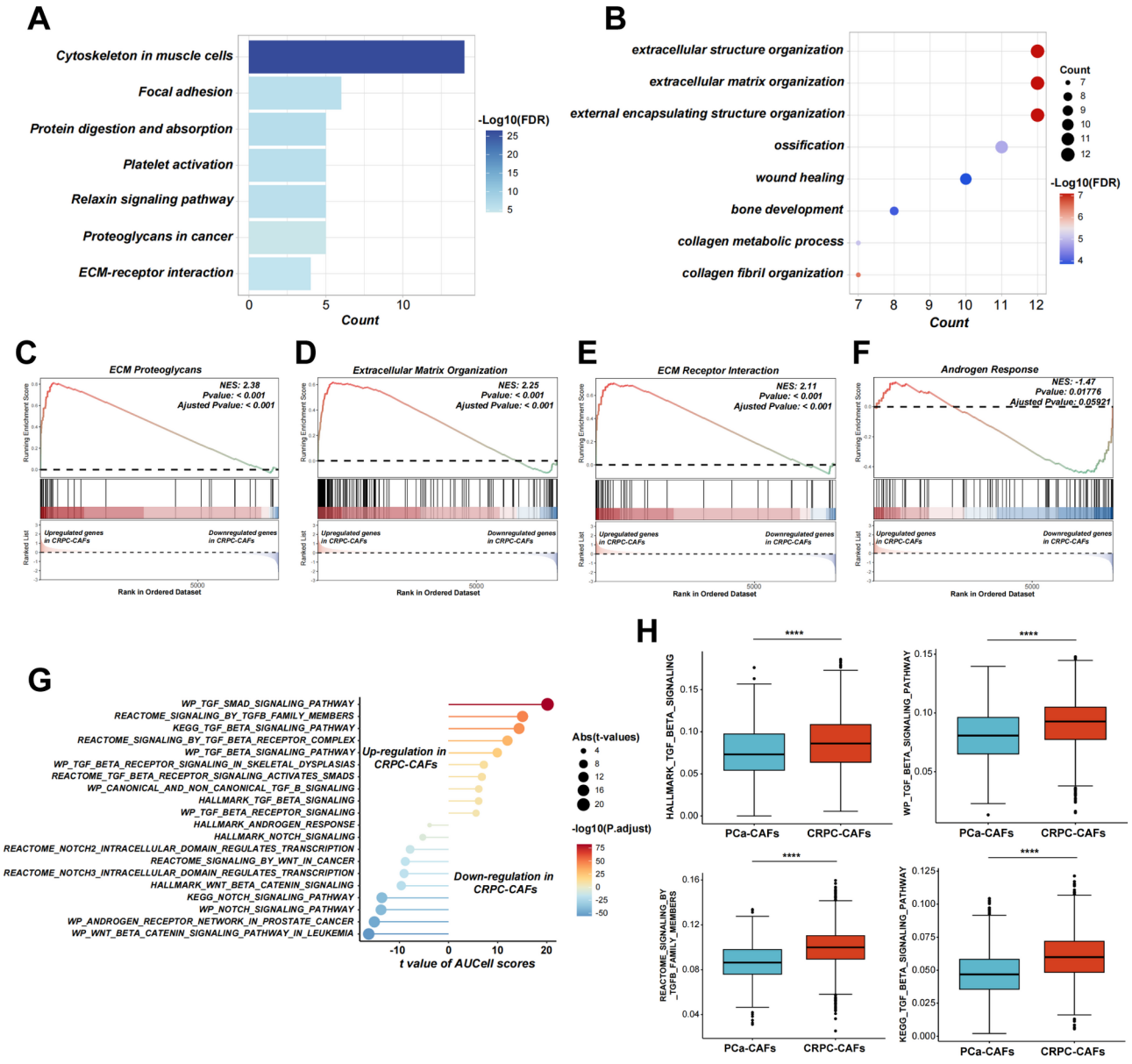

Fig. 2 Comprehensive analysis of the functional pathways within CRPC-CAFs. (**A**) Bar plot displaying significant enrichment of KEGG pathways of upregulated genes in CRPC-CAFs. (**B**) Dot plot displaying significant enrichment of GO pathways of upregulated genes in CRPC-CAFs. (**C-F**) GSEA results revealing upregulated and downregulated signaling pathways in CRPC-CAFs. (**G**) Lollipop Chart illustrating differential signaling pathways between CRPC-CAFs and PCa-CAFs. AUCell analysis was utilized to calculate activity scores of the signaling pathways. Comparison of AUCell scores between CRPC-CAFs and PCa-CAFs was achieved by Limma. t-values represent statistics computed by the fitting linear models. (**H**) Boxplot revealing a substantial upregulation of TGF-β-related signaling pathways. Statistical significance was assessed using a two-tailed Wilcoxon test. (*$p < 0.05$; **$p < 0.01$; ***$p < 0.001$; ****$p < 0.0001$.)

observations indicated that CAFs may play a substantial role in the reconfiguration of the TME, thereby potentially facilitating the progression to CRPC. However, the underlying transcriptional regulatory mechanisms that govern the phenotypic transition of CAFs remain to be elucidated.

PySCENIC analysis revealed significant differences in TFs activity between CRPC-CAFs and PCa-CAFs

To elucidate the transcriptional regulatory network in CRPC-CAFs, pySCENIC analysis was conducted to comprehensively analyze the transcription factor (TF) profiles in PCa-CAFs and CRPC-CAFs (Supplementary Table 3). First, the regulon specificity scores were calculated, and we found that POU3F3, PRRX2, GATA6, HOXB2, and PRDM6 were the most specific regulons in CAFs (Fig. 3F). Subsequently, we calculated TF activity

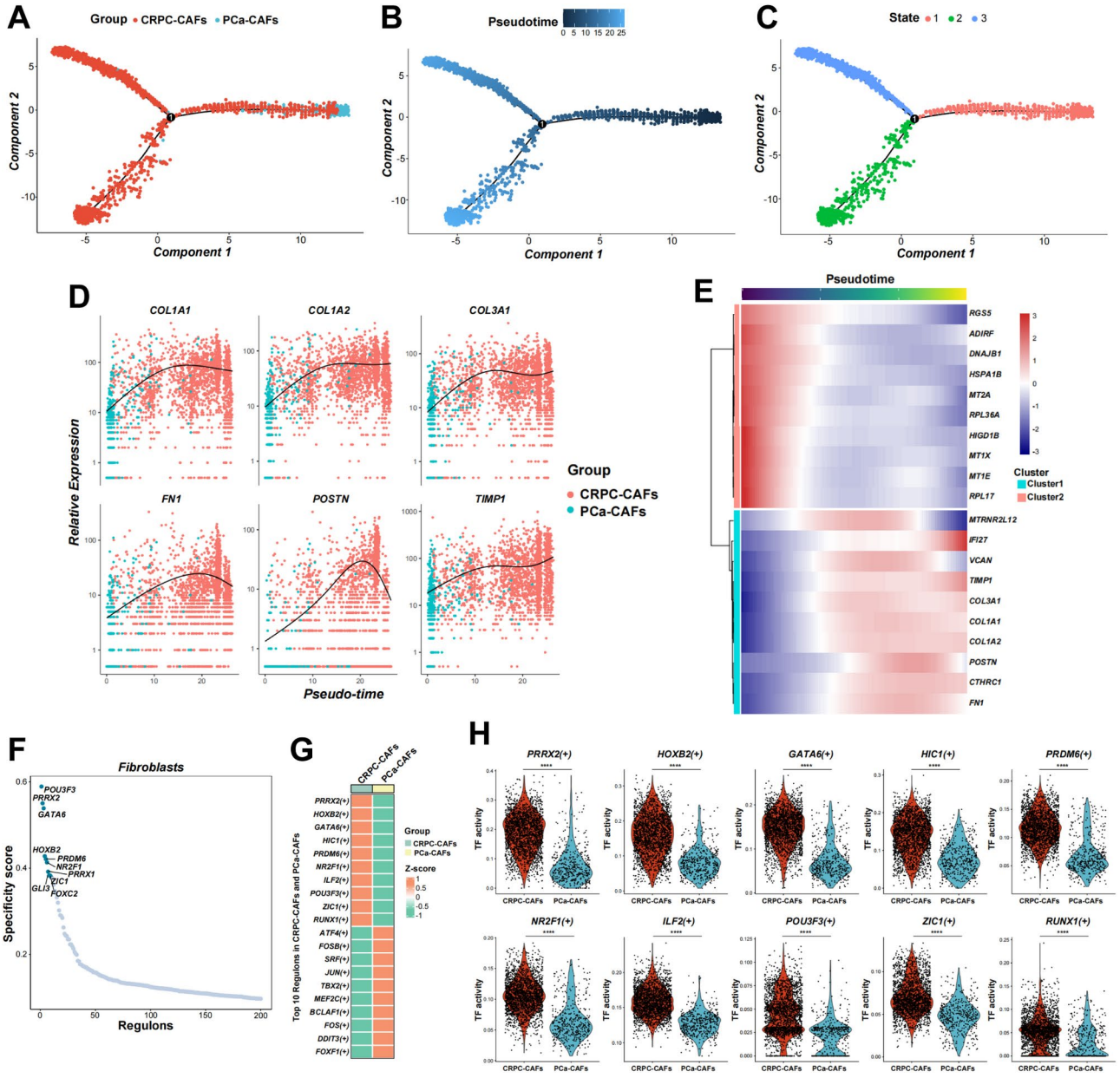

Fig. 3 Pseudotime and transcription factor analyses of CRPC-CAFs and PCa-CAFs. (**A-C**) Graphs illustrating the trajectories of CAFs, color-coded based on subgroup (**A**), pseudotime (**B**), and state (**C**). (**D**) Scatter plots presenting dynamic alterations in expression levels of marker genes of CRPC-CAFs, including COL1A1, COL1A2, COL3A1, FN1, POSTN, and TIMP1. (**E**) Heatmap illustrating the dynamic changes in expression of the top 10 DEGs between CRPC-CAFs and PCa-CAFs along the pseudotime. (**F**) Scatter plot revealing the most specific regulons in CAFs, as determined by regulon specificity score (RSS). (**G**) Heatmap displaying the scaled average activity scores of the top 10 differential regulons between CRPC-CAFs and PCa-CAFs. (**H**) Violin plots depicting a comparative analysis of regulon activity scores between CRPC-CAFs and PCa-CAFs. Statistical significance was assessed using a two-tailed Wilcoxon test. (*$p < 0.05$; **$p < 0.01$; ***$p < 0.001$; ****$p < 0.0001$.)

scores and employed limma to compare the differences in TF activity scores between PCa-CAFs and CRPC-CAFs (Supplementary Table 4). The top 10 most activated TFs in CRPC-CAFs and PCa-CAFs were shown in Fig. 3G. Notably, we observed that the transcriptional activity of PRRX2, HOXB2, GATA6, HIC1, PRDM6, NR2F1, ILF2, POU3F3, ZIC3, and RUNX1 was significantly elevated in CRPC-CAFs compared to PCa-CAFs (Fig. 3H). In summary, we discerned a specific set of TFs exhibiting markedly heightened transcriptional activity in CRPC-CAFs. This discovery suggests that these CRPC-CAFs-specific TFs may function as pivotal regulators in the malignant transformation of CAFs, and they may represent potential targets for preventing the progression to CRPC.

The differences in cell-cell interactions of CAFs with other cellular components between PCa and CRPC

To explore intercellular communication between CAFs and other cellular populations in the TME, CellChat was applied to establish a cell-cell interaction network and compare the differences between PCa and CRPC. We observed that the number and strength of intercellular interactions were significantly increased in CRPC compared to PCa (Supplementary Fig. 3A-B). Additionally, the differential interaction numbers and strengths of ligand-receptor signaling between CAFs and other cellular populations were markedly upregulated in CRPC compared to PCa (Supplementary Fig. 3C-D). These results demonstrated that the TME in CRPC exhibited a heightened complexity in intercellular interactions compared to that in primary PCa. CRPC-CAFs showed significantly upregulated TGF-β, FN1, CXCL12, and ANGPTL2 signaling by interacting with myeloid cells than PCa-CAFs (Supplementary Fig. 3E). In addition, the expression of VEGF, JAG1, FN1, CXCL12, ANGPTL2, and ANGPTL4 ligand-receptor pairs interacting with endothelial cells was markedly increased in CRPC-CAFs (Supplementary Fig. 3E). These data suggested that CAFs may modulate the functionality of myeloid cells and endothelial cells through paracrine signaling or direct cellular contact, thereby facilitating disease progression. Meanwhile, other cellular populations in the TME reciprocally modulate the function and behavior of CAFs. Myeloid cells showed a significantly increased expression of VCAM1, TGF-β, SPP1, PDGFB ligand-receptor pairs interacting with CAFs in CRPC compared with primary PCa (Supplementary Fig. 3F). The expression of TGF-β ligand-receptor pairs was markedly elevated in T cells, B cells, and endothelial cells by interacting with CAFs in CRPC (Supplementary Fig. 3F). Notably, the FN1-CD44 ligand-receptor interaction between CRPC-CAFs and T cells exhibited a significantly increased communication probability compared to other interactions. The probability of intercellular communication was calculated based on the expression levels of the ligand-receptor pair genes. Therefore, we further explored the expression of FN1 and CD44 in scRNA-seq data. Our results revealed a significant increase in the expression of FN1 in CRPC-CAFs compared to PCa-CAFs (Supplementary Fig. 4A-B). In contrast, the expression of CD44 in T cells did not exhibit a significant difference between CRPC and primary PCa (Supplementary Fig. 4C-D). These results indicated that the upregulated expression of FN1 in CRPC-CAFs contributed to markedly enhanced FN1-CD44 interaction in CRPC. Collectively, our findings suggested that the interactions between CAFs and other cellular components in the TME may contribute significantly to progression to CRPC.

TGF-β1 protein induced transcriptional and functional transformation of human prostatic fibroblasts

Our scRNA-seq analysis has uncovered a pronounced upregulation of the TGF-β signaling pathway within CRPC-CAFs. To validate these bioinformatics findings in vitro, we employed recombinant human TGF-β1 protein to treat the human prostatic fibroblast cell line WPMY-1. RT-qPCR analysis demonstrated that exogenous TGF-β1 protein treatment significantly upregulated the expression of genes implicated in ECM remodeling and TGF-β signaling, including FN1, TIMP1, COL1A1, TGFB1 and TGFB2 (Fig. 4A). However, expression of the transcription factor PRRX2 remained unchanged following TGF-β1 protein treatment, indicating that its elevated transcriptional activity in CRPC-CAFs may not correlate with expression levels. (Fig. 4A). The CCK-8 assay showed that TGF-β1 protein remarkably enhanced the proliferation capacity of WPMY-1 cells (Supplementary Fig. 5A). In addition, the wound healing assay showed that TGF-β1 treatment significantly facilitated the migration of WPMY-1 cells (Supplementary Fig. 5B). To comprehensively elucidate the impact of TGF-β1 on the biological functions of prostatic fibroblasts, RNA-seq was conducted on WPMY-1 cells. The principal component analysis (PCA) revealed a remarkable difference in the transcriptome profiles between WPMY-1 cells treated with TGF-β1 and those in the untreated group (Supplementary Fig. 5C). A total of 760 DEGs were identified, among which 167 genes exhibited pronounced upregulation in WPMY-1 cells treated with TGF-β1, whereas 593 genes were substantially downregulated (Fig. 4B; Supplementary Table 5). GSEA and ssGSEA results demonstrated that the TGF-β, MYC targets V1, MYC targets V2 and unfolded protein response signaling pathways were markedly activated in WPMY-1 cells treated with TGF-β1, whereas IFNα response, IFNγ response, inflammation and IL-6/JAK/STAT3 signaling pathways exhibited notable suppression (Fig. 4C-D). Our enrichment analyses revealed that the exogenous administration of TGF-β1 significantly activated prostatic fibroblasts, leading to an upregulation of the TGF-β signaling pathway and concomitant downregulation of immune response-associated pathways. Furthermore, we identified 6 genes that were commonly upregulated in both CRPC-CAFs and TGF-β1-treated prostatic fibroblasts, including TPM1, FN1, BGN, COL5A1, TNFAIP6 and CDH11 (Fig. 4E). The univariate Cox regression analysis of these 6 shared genes demonstrated that BGN is an independent risk factor intricately associated with RFS in PCa, as evidenced in both the TCGA and GSE21034 cohorts (Fig. 4F-G). Furthermore, Western blot analysis and RT-qPCR confirmed that the expression of BGN was significantly elevated in WPMY-1 cells treated with TGF-β1 (Fig. 4H; Supplementary Fig. 5D; Supplementary File 1). The

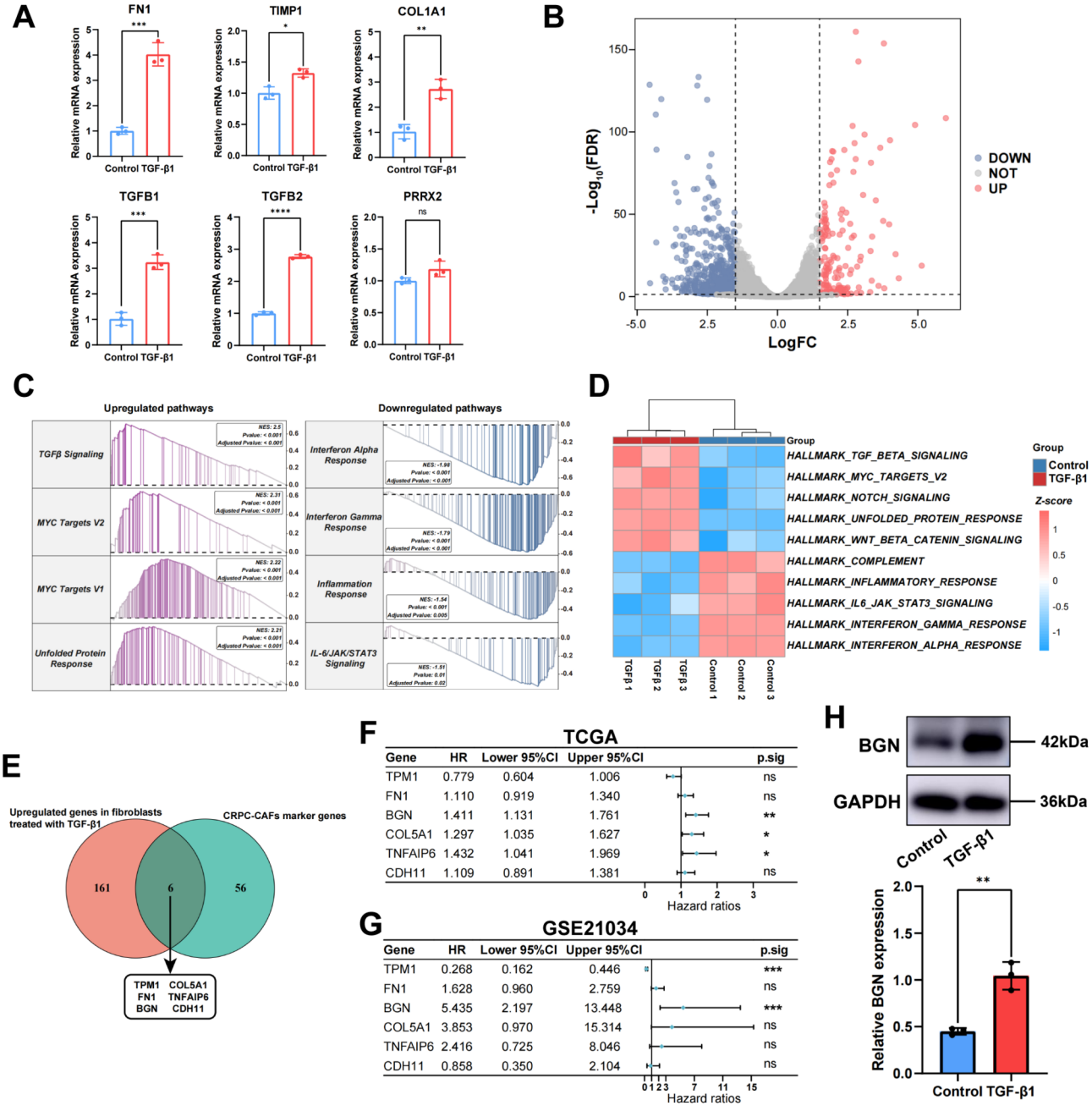

Fig. 4 TGF-β1 treatment exerting profound effects on human prostatic fibroblasts. (**A**) The RT-qPCR results for WPMY-1 cells treated with vehicle or TGF-β1. (**B**) Volcano plots displaying DEGs between WPMY-1 cells treated with vehicle or TGF-β1. (**C**) GSEA revealing significantly upregulated and downregulated signaling pathways in WPMY-1 cells treated with TGF-β1. (**D**) Heatmap displaying the activity levels of signaling pathways in WPMY-1 cells, as measured by ssGSEA. (**E**) Venn diagram illustrating the intersection of CRPC-CAFs marker genes and markedly upregulated genes in WPMY-1 cells treated with TGF-β1. (**F-G**) Forest plots displaying the results of univariate Cox regression analysis for the six genes in the TCGA (F) and GSE21034 (G) cohorts. (**H**) Immunoblotting analysis examining expression levels of BGN protein in WPMY-1 cells treated with vehicle or TGF-β1. Statistical significance was assessed using a two-tailed Student's t test. (*$p < 0.05$; **$p < 0.01$; ***$p < 0.001$; ****$p < 0.0001$.)

results suggested that BGN derived from activated CAFs may exert a pivotal effect on the progression of prostate cancer. In summary, exogenous administration of TGF-β1 protein could notably drive phenotypic and functional alterations in human prostatic fibroblasts.

CRPC-CAFs were associated with immunotherapy response and immunosuppressive TME

To examine the impact of CRPC-CAFs on the immune microenvironment in prostate cancer, we comprehensively analyzed the relationship between CRPC-CAFs abundance and immunotherapeutic response as well

as immune cells infiltration. In the IMvigor210 cohort, patients with higher CRPC-CAFs scores exhibited markedly shorter overall survival and a poorer immunotherapy response compared with those with lower scores (Fig. 5A-B). Notably, patients with higher CRPC-CAFs scores had significantly increased TIDE scores, indicating that CRPC-CAFs may promote immune evasion and resistance to immunotherapy (Fig. 5C). ESTIMATE analysis uncovered significantly increased immune scores and stromal scores in patients with higher CRPC-CAFs scores compared to those with lower scores (Supplementary Fig. 6A). CIBERSORT analysis showed that

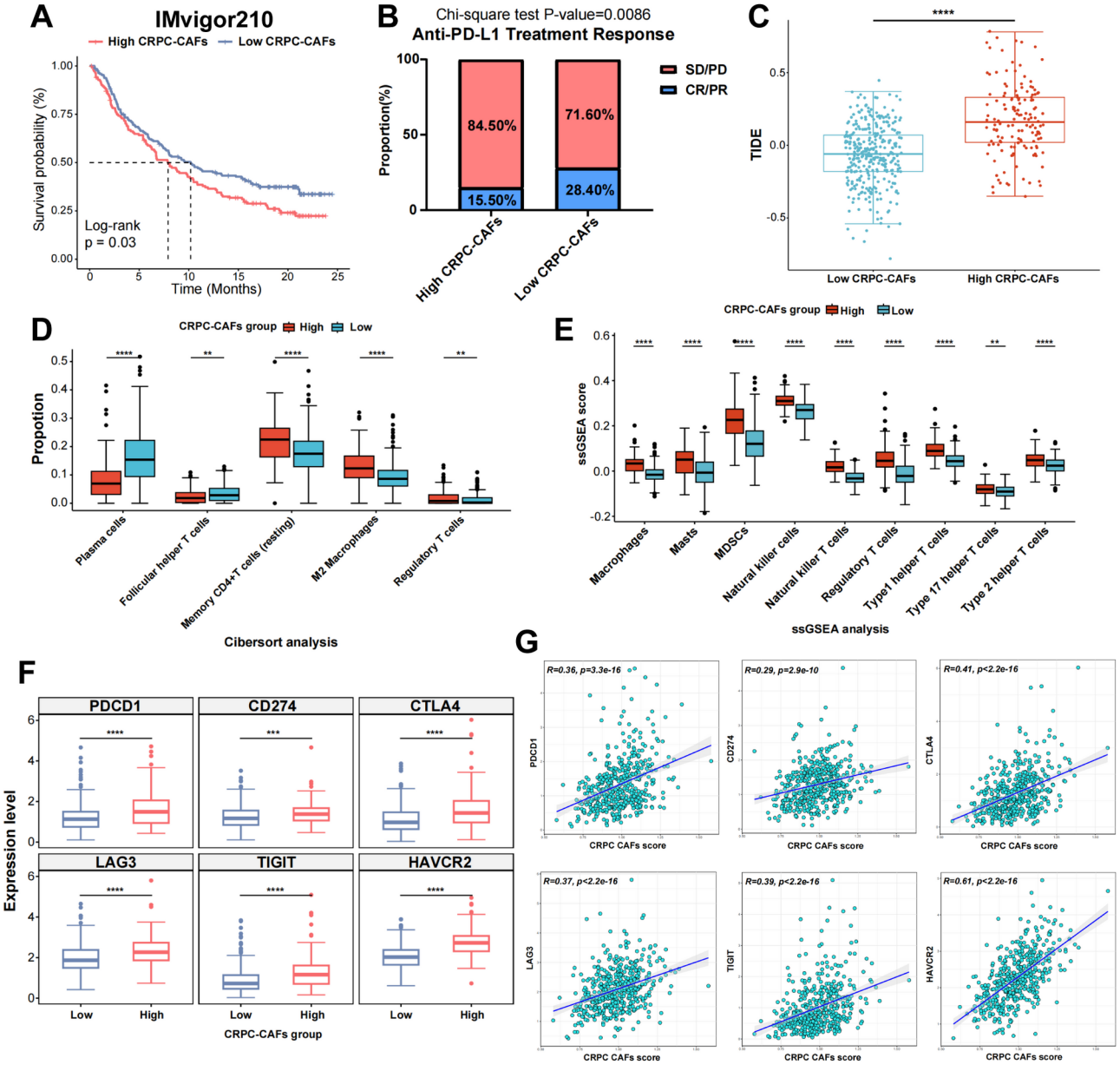

Fig. 5 The abundance of CRPC-CAFs correlating with immunotherapy response and the composition of the immune microenvironment. (**A**) Kaplan–Meier curves presenting a comparison of overall survival between patients with high versus low CRPC-CAFs scores in the IMvigor210 cohort. (**B**) Bar plot displaying a comparison of objective response rate of immunotherapy between patients with high versus low CRPC-CAFs scores in the IMvigor210 cohort. Statistical significance was assessed by utilizing a Chi-square test. (**C**) Boxplots illustrating a comparison of tumor immune dysfunction and exclusion (TIDE) score between patients with high versus low CRPC-CAFs scores. Statistical significance was assessed using a two-tailed Wilcoxon test. (*$p < 0.05$; **$p < 0.01$; ***$p < 0.001$; ****$p < 0.0001$.) (**D**) Boxplots presenting a comparative analysis of the proportion of intratumoral immune cells, as measured by CIBERSORT, between patients with high versus low CRPC-CAFs scores. (**E**) Boxplots presenting a comparative analysis of immune cell infiltration levels, as measured by ssGSEA, between patients with high versus low CRPC-CAFs scores. (**F**) Boxplots illustrating a comparison of the expression levels of immunosuppressive molecules between patients with high versus low CRPC-CAFs scores. (**G**) Spearman correlation analysis revealing markedly positive correlation between CRPC-CAFs scores and expression levels of immunosuppressive molecules, including PDCD1, CD274, CTLA4, LAG3, TIGIT, and HAVCR2

patients with high CRPC-CAFs scores had a markedly elevated proportion of memory $CD4^+$ T cells, Tregs, and M2 macrophages (Fig. 5D). Conversely, patients with low CRPC-CAFs scores displayed a notably increased relative abundance of plasma cells and follicular helper T cells (Fig. 5D). In addition, ssGSEA analysis revealed that the infiltration levels of macrophages, MDSCs, and regulatory T cells (Tregs) were significantly increased in patients with high CRPC-CAFs scores (Fig. 5E). To further decipher the relationship between CRPC-CAFs and other stromal cell densities in the TME, xCell analysis was conducted. The results revealed that patients with high CRPC-CAFs scores exhibited significantly higher densities of endothelial cells, fibroblasts, and pericytes compared to those with lower scores (Supplementary Fig. 6B). Our findings demonstrated that patients with high CRPC-CAFs scores exhibited remarkably increased infiltration of inhibitory immune cells and diminished efficacy of immunotherapy. Furthermore, we analyzed the correlation between CRPC-CAFs scores and expression of immunosuppressive molecules. Significantly increased expression of PDCD1, CD274, CTLA4, LAG3, TIGIT, and HAVCR2 was observed in patients with high CRPC-CAFs scores compared to those with lower scores (Fig. 5F). CRPC-CAFs scores showed a significantly positive correlation with the expression of PDCD1, CD274, CTLA4, LAG3, TIGIT, and HAVCR2 (Fig. 5G). In summary, these observations suggested that CRPC-CAFs may play a paramount role in establishing an immunosuppressive microenvironment, thereby contributing to resistance to immunotherapy in prostate cancer.

Blockade of TGF-β signaling augments the efficacy of immunotherapy in a murine model of PCa

Our aforementioned findings indicated that CRPC-CAFs, characterized by notable upregulation of TGF-β signaling, were intricately associated with resistance to immunotherapy. Additionally, ssGSEA analysis results demonstrated that the TGF-β signaling pathway was markedly activated in patients with high CRPC-CAFs scores (Fig. 6A). In addition to CRPC-CAFs, several other cell populations also exhibited pronounced upregulation of TGF-β signaling pathway in CRPC compared to primary PCa (Supplementary Fig. 7). Therefore, we hypothesized that blockade of TGF-β signaling could enhance the efficacy of immunotherapy in prostate cancer. To validate our hypothesis, we constructed a murine model of PCa with subcutaneously implanted RM-1 cells and treated with vehicle, anti-PD-1, anti-TGF-β or combination of anti-PD-1 and anti-TGF-β (Fig. 6B). We observed that, compared to the control group, mice in the anti-PD-1 or anti-TGF-β monotherapy group displayed significantly inhibited tumor growth (Fig. 6C-E). Moreover, the combination therapy of anti-PD-1 and anti-TGF-β exhibited remarkably synergistic inhibition of tumor growth (Fig. 6C-E). IHC staining demonstrated that the number of $CD4^+$ T cells and $CD8^+$ T cells was significantly increased in the combination therapy group compared with the anti-PD-1 or anti-TGF-β monotherapy group (Fig. 6F-H). To further investigate the effect of anti-TGF-β therapy on the TME of prostate cancer, we employed immunohistochemical staining to assess the expression levels of TGF-β1, α-SMA, PD-1, and PD-L1. Our results revealed a significant reduction in the expression of both TGF-β1 and α-SMA in the mice receiving anti-TGF-β monotherapy and combination therapy, as compared to the control group (Supplementary Fig. 8A-B). These results suggest that anti-TGF-β treatment markedly suppresses TGF-β signaling and the expression of TGF-β target genes in PCa mice. However, the expression levels of PD-1 and PD-L1 did not exhibit significant differences across the four experimental groups (Supplementary Fig. 8C-D). This observation suggests that anti-TGF-β therapy does not directly modulate the expression of PD-1 and PD-L1. Instead, anti-TGF-β treatment may exert an alternative influence on the TME, potentially facilitating the recruitment of immune cells and thereby augmenting the anti-tumor immune response. Collectively, these observations indicated that the inhibition of TGF-β signaling in CRPC-CAFs could enhance the efficacy of immunotherapeutic intervention through amplifying immune response in prostate cancer.

Discussion

Recent investigations have highlighted the profound influence of CAFs on cancer progression, metastasis, and drug resistance, which is exerted through both direct effects on tumor cells and indirect promotion of the immunosuppressive TME [37–40]. Nonetheless, the precise biological functions CAFs serve in the tumor milieu of CRPC have yet to be fully understood. Herein, we have delineated the tumor-promoting properties of CRPC-CAFs and validated their prognostic implications for clinical outcomes and responses to immunotherapy in prostate cancer.

With the rapid advancement and increasing application of sc-RNA-seq technology, we have a novel opportunity to decipher the heterogeneity in phenotypes and functions of distinct CAF subpopulations across a spectrum of cancer types [41]. For instance, a recent study uncovered a novel CAF subpopulation marked by elevated expression of PDGFRα and ITGA11, which plays a pivotal role in lymph node dissemination in early bladder cancer [42]. A subset of CAFs overexpressing SLC14A1 has been reported to confer chemoresistance and augment the stem-like characteristics of bladder cancer cells via the activation of WNT5A/β-catenin paracrine signaling [37]. Moreover, a recent single-cell analysis has

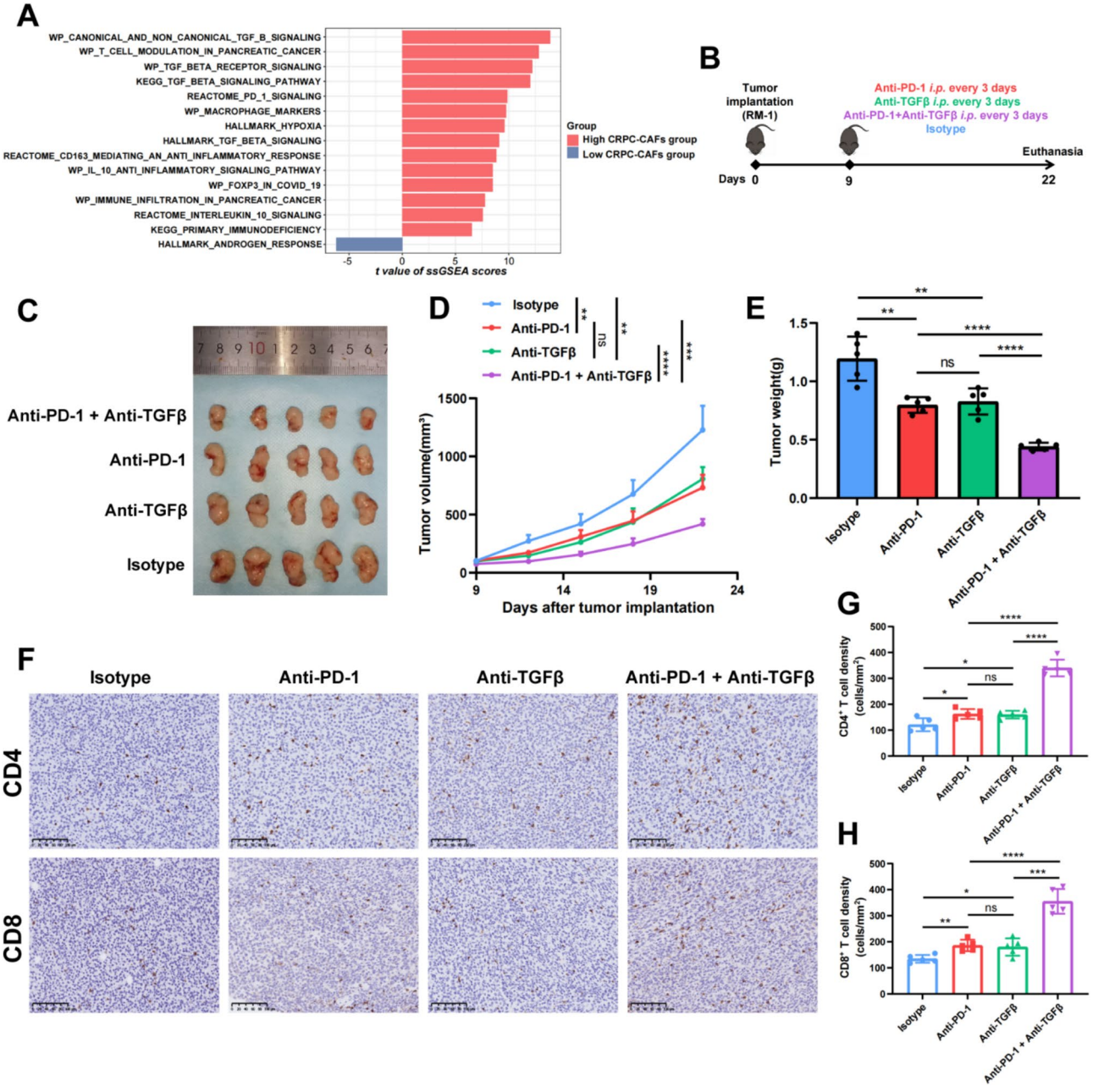

Fig. 6 Blockade of TGF-β signaling potentiating the efficacy of immunotherapeutic intervention. (**A**) Bar plot illustrating substantially upregulated signaling pathways in patients with high and low CRPC-CAFs abundance. Activity of signaling pathways was measured by ssGSEA. Comparison of ssGSEA activity scores between high and low CRPC-CAFs abundance groups was achieved by Limma. t-values represent statistics computed by the fitting linear models. (**B**) Schematic diagram illustrating experimental procedures and therapeutic administration strategy. (**C**) Gross appearance of the RM-1 tumors. (**D**) Tumor growth curves for mice bearing subcutaneous RM-1 implants following the administration of isotype IgG ($n=5$), anti-PD-1 ($n=5$), anti-TGF-β ($n=5$), and combination therapy of anti-PD-1 and anti-TGF-β ($n=5$). (**E**) Tumor weight of mice with subcutaneously implanted RM-1 tumors in distinct therapeutic groups. (**F**) Representative images of IHC staining of CD4 and CD8 in distinct therapeutic groups. Scale bars: 100 μm. (**G-H**) Quantitative analyses of the densities of $CD4^+$ T cells (G) and $CD8^+$ T cells (H) in distinct therapeutic groups. Statistical significance was assessed using a two-tailed Student's t test. (*$p<0.05$; **$p<0.01$; ***$p<0.001$; ****$p<0.0001$.)

revealed a TSPAN8-positive CAF subtype that contributes to resistance to chemotherapeutic agents in breast cancer by eliciting the degradation of SIRT6 and increasing the release of IL-6 and IL-8 [43]. Our scRNA-seq results uncovered significantly distinct transcriptomic profiles of CRPC-CAFs compared to those from primary PCa. Notably, CRPC-CAFs exhibited significant upregulation of the TGF-β signaling pathway and enhanced extracellular matrix remodeling. In line with our findings, a study also demonstrated that ADT can augment

activity of the TGF-β signaling pathway to facilitate the phenotypic transition of inflammatory CAFs to CRPC-CAFs, which accelerates resistance to ADT through increased paracrine secretion of SPP1 [44].

Through differential expression analysis and pseudotime trajectory analysis, we found a set of ECM-remodeling-associated genes was significantly upregulated in CRPC-CAFs compared to PCa-CAFs, including POSTN, FN1, COL1A1, and TIMP1. Consistent with our results, a previous report demonstrated that the expression level of POSTN was markedly elevated in metastatic CRPC (mCRPC) tissues compared to that in primary PCa tissues [45]. Additionally, elevated plasma levels of POSTN were positively correlated with unfavorable clinical outcomes in patients with mCRPC. Recently, POSTN-positive CAFs have been reported to be intricately implicated in T cell functional exhaustion in the TME, eventually leading to a more unfavorable clinical prognosis in patients with non-small cell lung cancer [46]. Similarly, a separate study identified a CAF subpopulation with elevated POSTN expression that facilitates tumor progression and confers resistance to immunotherapy in hepatocellular cancer [47]. Our in vitro experimental findings confirm that the expression levels of ECM-remodeling-related genes, such as FN1, COL1A1, and TIMP1, are markedly elevated in human prostatic fibroblasts following exposure to TGF-β1 protein. It has been reported that FN1 is implicated in tumor progression and poor clinical prognosis in various cancers including breast cancer, thyroid cancer, and esophageal squamous cell carcinoma [48–50]. COL1A1 and TIMP1, as pivotal components of the extracellular matrix, also play important roles in the process of cancer progression and metastasis [51–54]. Therefore, targeted inhibition of CRPC-CAFs could represent a promising therapeutic strategy to prevent progression of prostate cancer. Notably, the gene BGN, which is markedly upregulated in TGF-β1-treated prostatic fibroblasts, has been found to be positively associated with unfavorable clinical outcomes in prostate cancer. In line with our findings, a recent study has uncovered that BGN, as a secretory proteoglycan predominantly derived from CAFs, is implicated in unfavorable prognosis and resistance to immunotherapeutic interventions across a spectrum of malignancies [55]. In breast cancer, CAF-derived BGN is reported to be closely correlated with adverse prognosis and the immunosuppressive tumor milieu, particularly characterized by a diminished infiltration of $CD8^+$ T cells [56]. Employing proteomic analysis, a recent investigation has disclosed that the BGN protein serves as a predictive biomarker for the transition from HSPC to CRPC [57].

Transcription factors have been recognized as critical modulators of molecular and functional heterogeneity among distinct CAF subpopulations [58]. Our findings indicate that PRRX2 may hold an indispensable role in driving the transition of PCa-CAFs to CRPC-CAFs. PRRX2, as a transcription factor intricately implicated in cellular differentiation and oncogenic processes, exhibits remarkable upregulation in response to TGF-β signaling, subsequently facilitating breast cancer progression and EMT [59]. Recently, PRRX2 has been reported to function as a critical factor eliciting resistance to androgen-receptor inhibitors, mediated by marked upregulation of RB1/E2F and BCL2 signaling [60]. In light of the aforementioned results, further experimental investigation is warranted to elucidate the regulatory function of PRRX2 in CRPC-CAFs.

Utilizing CellChat analysis, we observed remarkably enhanced interaction of the FN1-CD44 ligand-receptor pair between CRPC-CAFs and T cells. Consistent with our findings, a recent study has revealed that CAFs exhibited markedly enhanced interactions with T cells and myeloid cells via the FN1-CD44 signaling axis, thereby facilitating invasion and metastasis in colorectal cancer [61]. FN1, a critical glycoprotein component of the extracellular matrix in the TME, exerts profound effects on tumor cell proliferation, invasion, and ECM remodeling [62–64]. The expression of FN1 is intricately correlated with clinical prognosis and immune cell infiltration in various cancers [65, 66]. CD44 is widely recognized as a marker of cancer stem cells in human malignancies and has been reported to be implicated in unfavorable prognosis, drug resistance, and immune evasion [67, 68]. Recent research has uncovered that CD44 is capable of upregulating the expression of PD-L1 in breast and lung cancers [69]. Given these findings, it is essential to assess the strength of the FN1-CD44 interaction between CAFs and T cells in CRPC and to determine the effect of this interaction on tumor progression in transgenic models of spontaneous prostate cancer in the future.

Importantly, our data uncovered that patients with high CRPC-CAFs abundance exhibited diminished sensitivity to immune checkpoint inhibitors. Recently, mounting evidence has demonstrated that CAFs can interact with diverse immune cell populations in the TME, exerting a profound influence on anti-tumor immune response [70]. WNT2, derived from CAFs, has emerged as a pivotal modulator of the phenotype and biological functions of dendritic cells (DCs) within the TME [71]. In addition, the blockade of WNT2 signaling dramatically potentiates the efficacy of immunotherapeutic interventions through augmenting anti-tumor immune response. In the context of breast cancer (BC), CAFs are significantly implicated in the diminished frequency of $CD8^+$ T cells and unresponsiveness to immunotherapy [72]. In alignment with their findings, our research indicates that CRPC-CAFs are intricately associated with the creation of an immunosuppressive tumor milieu, characterized by elevated

abundance of inhibitory immune cells and upregulated expression of immunosuppressive molecules.

A burgeoning body of evidence sheds light on the paramount role of TGF-β signaling in modulating the functions of diverse immune cell populations and affecting responsiveness to immunotherapy [73, 74]. Herein, we discerned a marked activation of TGF-β and immune evasion-related signaling pathways in patients with high abundance of CRPC-CAFs. Leveraging a subcutaneous PCa tumor-bearing model, our study demonstrated that blockade of TGF-β signaling significantly potentiated the efficacy of anti-PD-1 immunotherapy and elicited a substantial increase in the density of both $CD4^+$ and $CD8^+$ T cells. Consistent with our data, recent studies have revealed that the combination of immunotherapeutic interventions and specific inhibition of TGF-β signaling substantially restrains tumor progression and metastasis, mediated by an increase in the frequency of T cells and activation of their biological functions [75–77]. Furthermore, interrupting the TGF-β signaling cascade can augment cytotoxic potential of NK cells, subsequently facilitating the regression of bladder cancer [78].

There exist several limitations in our present study that warrant further improvement. Genetically engineered mice with fibroblast-specific conditional gene manipulation allow for a more precise elucidation of the impact of CRPC-CAFs on the tumor immune milieu and immunotherapy response. Furthermore, large-scale, multi-center cohorts are warranted to validate the prognostic implications of the abundance of CRPC-CAFs. Finally, there is a need to isolate primary CAFs from CRPC tissues to explore the molecular mechanisms by which CRPC-CAFs interact with immune cells.

Taken together, we uncover a subpopulation of CRPC-CAFs intricately associated with unfavorable clinical outcomes and insensitivity to immunotherapeutic agents. Moreover, the elevated abundance of CRPC-CAFs is involved in the upregulation of TGF-β signaling and immunosuppression in PCa. Our findings propose that targeting CRPC-CAFs may represent a promising therapeutic strategy for improving prognosis and the efficacy of immunotherapy in patients with CRPC.

Supplementary Information

The online version contains supplementary material available at https://doi.org/10.1186/s12885-025-14212-x.

Supplementary Fig. 1: (**A**) t-SNE plot of 33 different single-cell clusters. (**B**) Dot plot comparing the average expression levels of several epithelial cell marker genes, including KRT8, KRT18, AR, and KLK3, between epithelial cells and fibroblasts. (**C-D**) Boxplots illustrating a comparison of CRPC-CAFs signature scores between localized PCa and metastatic CRPC tissues in the GSE32269 (C) and GSE70768 (D) cohorts

Supplementary Fig. 2: (A-D): Leading-edge analysis of GSEA identified the core enriched genes in signaling pathways, including ECM proteoglycans (A), ECM organization (B), ECM receptor interaction (C), and androgen response (D)

Supplementary Fig. 3: Intercellular interaction analysis of CAFs and other cell types in PCa and CRPC. (**A**) Bar plots presenting the number and strength of intercellular interactions in PCa and CRPC. (**B**) Network plots illustrating the number of intercellular interactions between distinct cell types within the TME of PCa and CRPC. (**C**) Heatmaps displaying the differential number and strength of intercellular interactions between PCa and CRPC. Red color denotes elevation of the differential number and strength of interactions in CRPC compared with PCa, whereas blue color indicates reduction of the differential number and strength of interactions in CRPC compared with PCa. (**D**) Network plots illustrating the differential number and strength of intercellular interactions between PCa and CRPC. The red arrowed line indicates a significant increase in the differential number and strength of interactions in CRPC in comparison with PCa, whereas the blue arrowed line signifies diminished differential number and strength of interactions. (**E**) Dot plots comparing communication probabilities of the major ligand-receptor pairs from CAFs to other cell components in the TME between PCa and CRPC (**F**) Dot plots comparing communication probabilities of the major ligand-receptor pairs from distinct cellular components to CAFs in the TME between PCa and CRPC

Supplementary Fig. 4: (A): t-SNE plot displaying the expression level of FN1 in CRPC and primary PCa. (**B**) Violin plot comparing the expression of FN1 between CAFs derived from CRPC and primary PCa. (**C**) t-SNE plot displaying the expression level of CD44 in CRPC and primary PCa. (**D**) Violin plot comparing the expression of CD44 between T cells derived from CRPC and primary PCa. Statistical significance was assessed using a two-tailed Student's t test. (*$p < 0.05$; **$p < 0.01$; ***$p < 0.001$; ****$p < 0.0001$.)

Supplementary Fig. 5: (**A**) The CCK-8 assay was employed to evaluate the proliferative capacity of WPMY-1 cells treated with vehicle or TGF-β1. (**B**) The scratch healing assay was utilized to assess the migration of WPMY-1 cells treated with vehicle or TGF-β1. (**C**) PCA scatter plot comparing the transcriptome profiles between WPMY-1 cells treated with TGF-β1 and those in the control group. (**D**) RT-qPCR analysis of BGN mRNA expression in WPMY-1 cells following treatment with vehicle or TGF-β1

Supplementary Fig. 6: (**A**) Boxplots presenting a comparison of immune score, stromal score and tumor purity between patients with high versus low CRPC-CAFs signature scores. (**B**) Boxplots presenting a comparative analysis of the abundance of stromal cells in the TME, as assessed by Xcell algorithm, between patients with high versus low CRPC-CAFs signature scores

Supplementary Fig. 7: Boxplots presenting a comparison of AUCell activity scores of the TGF-β signaling pathway across distinct cell types between PCa and CRPC. Statistical significance was assessed using a two-tailed Wilcoxon test. (*$p < 0.05$; **$p < 0.01$; ***$p < 0.001$; ****$p < 0.0001$.)

Supplementary Fig. 8: immunohistochemistry staining and quantification of TGF-β1, α-SMA, PD-1, PD-L1 in PCa murine model. Representative IHC staining images of TGF-β1 (A), α-SMA (B), PD-1 (C), and PD-L1 (D) in four different therapeutic groups. Scale bars: 100 μm. For quantitative analysis, the percentage area (%Area) of positive staining was determined by utilizing ImageJ software. Statistical significance was assessed using a two-tailed Student's t test. (*$p < 0.05$; **$p < 0.01$; ***$p < 0.001$; ****$p < 0.0001$.)

Supplementary Table 1: The primers for RT-qPCR

Supplementary Table 2: The marker genes significantly upregulated in CRPC-CAFs and PCa-CAFs

Supplementary Table 3: The regulons identified by using pySCENIC analysis, including transcription factors (TFs) and their corresponding target genes

Supplementary Table 4: The AUCell scores of regulons in CAFs derived from PCa and CRPC

Supplementary Table 5: The results of differential expression analysis between WPMY-1 cells treated with TGF-β1 and those in the control group

Supplementary File 1: The original, unprocessed immunoblot images of our manuscript

Supplementary File 2: The description of mice euthanasia methods

Acknowledgements
Not applicable.

Author contributions
QH, BHL were responsible for the conceptualization and design of the study. YFQ contributed to the bioinformatics analysis and data interpretation. YFQ and YHW performed the experiments and statistical analyses. YFQ and JHL contributed to the acquisition of publicly available data and the preparation of figures for the manuscript. YFQ contributed to drafting the manuscript. QH, BHL, KS contributed to revising and editing the manuscript. Each author has read and approved the final version of the manuscript to be published.

Funding
This work was supported by Shenzhen International Cooperation Research Project (GJHZ20220913143004008); HaiYa Young Scientist Foundation of Shenzhen University General Hospital; National Natural Science Foundation of China (82002716);; Shenzhen Scientific Research Foundation for Excellent Returned Scholars (000493); Natural Science Foundation of Shenzhen University General Hospital (SUGH2020QD005); Disciple gathering teaching project of Shenzhen University; Shenzhen Key Laboratory Foundation (ZDSYS20200811143757022); Teaching Reform Research Project of Shenzhen University (YXBJG202339); Educational Reform Research Project of Clinical Teaching Base of Guangdong Province (2021JD207); Medical and Health Science and Technology Project (support) of Longgang District, Shenzhen (LGKCYLWS2021000032); Key Project of Medical and health technology of Longgang District, Shenzhen (LGKCYLWS2022034); Shenzhen Municipal Commission of Science and Technology Innovation (JCYJ20220818100009020, JCYJ20220818100016035).

Data availability
The scRNA-seq datasets (GSE141445 and GSE210358) and Affymetrix microarray data (GSE70769, GSE21034, GSE32269, and GSE70768) are accessible in the Gene Expression Omnibus (GEO) repository (https://www.ncbi.nlm.nih.gov/geo). Furthermore, the bulk RNA-seq data encompassed datasets from TCGA-PRAD (http://xena.ucsc.edu/) and IMvigor210 (http://research-pub.gene.com/IMvigor210CoreBiologies) cohorts. The raw bulk RNA-seq data generated in this study have been deposited in the Sequence Read Archive (SRA) repository under the accession number PRJNA1169197.

Declarations

Ethics approval and consent to participate
Not applicable.

Consent for publication
Not applicable.

Competing interests
The authors declare no competing interests.

Author details
[1]Guangdong Key Laboratory for Biomedical Measurements and Ultrasound Imaging, National-Regional Key Technology Engineering Laboratory for Medical Ultrasound, School of Biomedical Engineering, Shenzhen University Medical school, Shenzhen 518060, China
[2]Department of Urology, Shenzhen University General Hospital, Shenzhen University, Shenzhen, Guangdong, China
[3]Shenzhen Key Laboratory for Systemic Aging and Intervention (SAI), Guangdong Key Laboratory of Genome Stability and Human Disease Prevention, School of Basic Medical Sciences, Marshall Laboratory of Biomedical Engineering, National Engineering Research Center for Biotechnology (Shenzhen), International Cancer Center, Shenzhen University, Shenzhen, Guangdong, China
[4]Department of Radiology, the Third People's Hospital of Longgang District, Shenzhen, China
[5]Shenzhen Clinical Medical School, Guangzhou University of Chinese Medicine, Shenzhen 518116, China
[6]International Cancer Center, Shenzhen Key Laboratory, Hematology Institution of Shenzhen University, Shenzhen, China

Received: 4 October 2024 / Accepted: 23 April 2025
Published online: 30 April 2025

References

1. Bray F, Laversanne M, Sung H, Ferlay J, Siegel RL, Soerjomataram I, et al. Global cancer statistics 2022: GLOBOCAN estimates of incidence and mortality worldwide for 36 cancers in 185 countries. CA Cancer J Clin. 2024;74:229–63.
2. Karantanos T, Corn PG, Thompson TC. Prostate cancer progression after androgen deprivation therapy: mechanisms of castrate resistance and novel therapeutic approaches. Oncogene. 2013;32:5501–11.
3. Chandrasekar T, Yang JC, Gao AC, Evans CP. Mechanisms of resistance in castration-resistant prostate cancer (CRPC). Transl Androl Urol. 2015;4:365–80.
4. Harris WP, Mostaghel EA, Nelson PS, Montgomery B. Androgen deprivation therapy: progress in Understanding mechanisms of resistance and optimizing androgen depletion. Nat Clin Pract Urol. 2009;6:76–85.
5. Cornford P, van den Bergh RCN, Briers E, Van den Broeck T, Cumberbatch MG, De Santis M, et al. EAU-EANM-ESTRO-ESUR-SIOG guidelines on prostate cancer. Part II-2020 update: treatment of relapsing and metastatic prostate Cancer. Eur Urol. 2021;79:263–82.
6. Drake CG, Sharma P, Gerritsen W. Metastatic castration-resistant prostate cancer: new therapies, novel combination strategies and implications for immunotherapy. Oncogene. 2014;33:5053–64.
7. Kallio HML, Hieta R, Latonen L, Brofeldt A, Annala M, Kivinummi K, et al. Constitutively active androgen receptor splice variants AR-V3, AR-V7 and AR-V9 are co-expressed in castration-resistant prostate cancer metastases. Br J Cancer. 2018;119:347–56.
8. Watson PA, Arora VK, Sawyers CL. Emerging mechanisms of resistance to androgen receptor inhibitors in prostate cancer. Nat Rev Cancer. 2015;15:701–11.
9. Lu X, Horner JW, Paul E, Shang X, Troncoso P, Deng P, et al. Effective combinatorial immunotherapy for castration-resistant prostate cancer. Nature. 2017;543:728–32.
10. Calcinotto A, Spataro C, Zagato E, Di Mitri D, Gil V, Crespo M, et al. IL-23 secreted by myeloid cells drives castration-resistant prostate cancer. Nature. 2018;559:363–9.
11. Zhang Y, Fan A, Li Y, Liu Z, Yu L, Guo J, et al. Single-cell RNA sequencing reveals that HSD17B2 in cancer-associated fibroblasts promotes the development and progression of castration-resistant prostate cancer. Cancer Lett. 2023;566:216244.
12. Dg ESIAEC, Rm DME. E, A framework for advancing our Understanding of cancer-associated fibroblasts. Nat Rev Cancer. 2020;20.
13. Friedman G, Levi-Galibov O, David E, Bornstein C, Giladi A, Dadiani M, et al. Cancer-associated fibroblast compositions change with breast cancer progression linking the ratio of S100A4 + and PDPN + CAFs to clinical outcome. Nat Cancer. 2020;1:692–708.
14. Monteran L, Erez N. The dark side of fibroblasts: Cancer-Associated fibroblasts as mediators of immunosuppression in the tumor microenvironment. Front Immunol. 2019;10:1835.
15. Cheteh EH, Augsten M, Rundqvist H, Bianchi J, Sarne V, Egevad L, et al. Human cancer-associated fibroblasts enhance glutathione levels and antagonize drug-induced prostate cancer cell death. Cell Death Dis. 2017;8:e2848.
16. Sun Y, Campisi J, Higano C, Beer TM, Porter P, Coleman I, et al. Treatment-induced damage to the tumor microenvironment promotes prostate cancer therapy resistance through WNT16B. Nat Med. 2012;18:1359–68.
17. Z Z, Wr K, Ys L, Vr G, C W, Jw R et al. Tumor Microenvironment-Derived NRG1 promotes antiandrogen resistance in prostate Cancer. Cancer Cell. 2020;38.
18. Enriquez C, Cancila V, Ferri R, Sulsenti R, Fischetti I, Milani M, et al. Castration-Induced downregulation of SPARC in stromal cells drives neuroendocrine differentiation of prostate Cancer. Cancer Res. 2021;81:4257–74.
19. Cui D, Li J, Zhu Z, Berk M, Hardaway A, McManus J, et al. Cancer-associated fibroblast-secreted glucosamine alters the androgen biosynthesis program in prostate cancer via HSD3B1 upregulation. J Clin Invest. 2023;133:e161913.
20. Chen S, Zhu G, Yang Y, Wang F, Xiao Y-T, Zhang N, et al. Single-cell analysis reveals transcriptomic remodellings in distinct cell types that contribute to human prostate cancer progression. Nat Cell Biol. 2021;23:87–98.
21. Bian X, Wang W, Abudurexiti M, Zhang X, Ma W, Shi G, et al. Integration analysis of Single-Cell Multi-Omics reveals prostate Cancer heterogeneity. Adv Sci (Weinh). 2024;11:e2305724.
22. Chan JM, Zaidi S, Love JR, Zhao JL, Setty M, Wadosky KM, et al. Lineage plasticity in prostate cancer depends on JAK/STAT inflammatory signaling. Science. 2022;377:1180–91.

23. Korsunsky I, Millard N, Fan J, Slowikowski K, Zhang F, Wei K, et al. Fast, sensitive and accurate integration of single-cell data with harmony. Nat Methods. 2019;16:1289–96.
24. Luo H, Xia X, Huang L-B, An H, Cao M, Kim GD, et al. Pan-cancer single-cell analysis reveals the heterogeneity and plasticity of cancer-associated fibroblasts in the tumor microenvironment. Nat Commun. 2022;13:6619.
25. Dong B, Miao J, Wang Y, Luo W, Ji Z, Lai H, et al. Single-cell analysis supports a luminal-neuroendocrine transdifferentiation in human prostate cancer. Commun Biol. 2020;3:778.
26. Henry GH, Malewska A, Joseph DB, Malladi VS, Lee J, Torrealba J, et al. A cellular anatomy of the normal adult human prostate and prostatic urethra. Cell Rep. 2018;25:3530–e35425.
27. Wu T, Hu E, Xu S, Chen M, Guo P, Dai Z, et al. ClusterProfiler 4.0: A universal enrichment tool for interpreting omics data. Innov (Camb). 2021;2:100141.
28. Liberzon A, Birger C, Thorvaldsdóttir H, Ghandi M, Mesirov JP, Tamayo P. The molecular signatures database (MSigDB) hallmark gene set collection. Cell Syst. 2015;1:417–25.
29. Aibar S, González-Blas CB, Moerman T, Huynh-Thu VA, Imrichova H, Hulselmans G, et al. SCENIC: single-cell regulatory network inference and clustering. Nat Methods. 2017;14:1083–6.
30. Qiu X, Mao Q, Tang Y, Wang L, Chawla R, Pliner HA, et al. Reversed graph embedding resolves complex single-cell trajectories. Nat Methods. 2017;14:979–82.
31. Jin S, Guerrero-Juarez CF, Zhang L, Chang I, Ramos R, Kuan C-H, et al. Inference and analysis of cell-cell communication using cellchat. Nat Commun. 2021;12:1088.
32. Yoshihara K, Shahmoradgoli M, Martínez E, Vegesna R, Kim H, Torres-Garcia W, et al. Inferring tumour purity and stromal and immune cell admixture from expression data. Nat Commun. 2013;4:2612.
33. Newman AM, Steen CB, Liu CL, Gentles AJ, Chaudhuri AA, Scherer F, et al. Determining cell type abundance and expression from bulk tissues with digital cytometry. Nat Biotechnol. 2019;37:773–82.
34. Charoentong P, Finotello F, Angelova M, Mayer C, Efremova M, Rieder D, et al. Pan-cancer Immunogenomic analyses reveal Genotype-Immunophenotype relationships and predictors of response to checkpoint Blockade. Cell Rep. 2017;18:248–62.
35. Aran D, Hu Z, Butte AJ. xCell: digitally portraying the tissue cellular heterogeneity landscape. Genome Biol. 2017;18:220.
36. Jiang P, Gu S, Pan D, Fu J, Sahu A, Hu X, et al. Signatures of T cell dysfunction and exclusion predict cancer immunotherapy response. Nat Med. 2018;24:1550–8.
37. Ma Z, Li X, Mao Y, Wei C, Huang Z, Li G, et al. Interferon-dependent SLC14A1 + cancer-associated fibroblasts promote cancer stemness via WNT5A in bladder cancer. Cancer Cell. 2022;40:1550–e15657.
38. Neuwirt H, Bouchal J, Kharaishvili G, Ploner C, Jöhrer K, Pitterl F, et al. Cancer-associated fibroblasts promote prostate tumor growth and progression through upregulation of cholesterol and steroid biosynthesis. Cell Commun Signal. 2020;18:11.
39. Li C, Guo H, Zhai P, Yan M, Liu C, Wang X, et al. Spatial and Single-Cell transcriptomics reveal a Cancer-Associated fibroblast subset in HNSCC that restricts infiltration and antitumor activity of CD8 + T cells. Cancer Res. 2024;84:258–75.
40. Jia D, Zhou Z, Kwon O-J, Zhang L, Wei X, Zhang Y, et al. Stromal FOXF2 suppresses prostate cancer progression and metastasis by enhancing antitumor immunity. Nat Commun. 2022;13:6828.
41. Lavie D, Ben-Shmuel A, Erez N, Scherz-Shouval R. Cancer-associated fibroblasts in the single-cell era. Nat Cancer. 2022;3:793–807.
42. Zheng H, An M, Luo Y, Diao X, Zhong W, Pang M, et al. PDGFRα + ITGA11 + fibroblasts foster early-stage cancer lymphovascular invasion and lymphatic metastasis via ITGA11-SELE interplay. Cancer Cell. 2024;42:682–e70012.
43. Fan G, Yu B, Tang L, Zhu R, Chen J, Zhu Y, et al. TSPAN8 + myofibroblastic cancer-associated fibroblasts promote chemoresistance in patients with breast cancer. Sci Transl Med. 2024;16:eadj5705.
44. Wang H, Li N, Liu Q, Guo J, Pan Q, Cheng B, et al. Antiandrogen treatment induces stromal cell reprogramming to promote castration resistance in prostate cancer. Cancer Cell. 2023;41:1345–e13629.
45. Cattrini C, Barboro P, Rubagotti A, Zinoli L, Zanardi E, Capaia M, et al. Integrative analysis of Periostin in primary and advanced prostate Cancer. Transl Oncol. 2020;13:100789.
46. Chen C, Guo Q, Liu Y, Hou Q, Liao M, Guo Y, et al. Single-cell and Spatial transcriptomics reveal POSTN + cancer-associated fibroblasts correlated with immune suppression and tumour progression in non-small cell lung cancer. Clin Transl Med. 2023;13:e1515.
47. Wang H, Liang Y, Liu Z, Zhang R, Chao J, Wang M, et al. POSTN + cancer-associated fibroblasts determine the efficacy of immunotherapy in hepatocellular carcinoma. J Immunother Cancer. 2024;12:e008721.
48. Chen C, Ye L, Yi J, Liu T, Li Z. FN1 mediated activation of aspartate metabolism promotes the progression of triple-negative and luminal a breast cancer. Breast Cancer Res Treat. 2023;201:515–33.
49. Chen C, Shen Z. FN1 promotes thyroid carcinoma cell proliferation and metastasis by activating the NF-Kb pathway. Protein Pept Lett. 2023;30:54–64.
50. Ma J, Chen S, Su M, Wang W. High FN1 expression is associated with poor survival in esophageal squamous cell carcinoma. Med (Baltim). 2023;102:e33388.
51. Liu J, Shen J-X, Wu H-T, Li X-L, Wen X-F, Du C-W, et al. Collagen 1A1 (COL1A1) promotes metastasis of breast cancer and is a potential therapeutic target. Discov Med. 2018;25:211–23.
52. Li M, Wang J, Wang C, Xia L, Xu J, Xie X, et al. Microenvironment remodeled by tumor and stromal cells elevates fibroblast-derived COL1A1 and facilitates ovarian cancer metastasis. Exp Cell Res. 2020;394:112153.
53. Song G, Xu S, Zhang H, Wang Y, Xiao C, Jiang T, et al. TIMP1 is a prognostic marker for the progression and metastasis of colon cancer through FAK-PI3K/AKT and MAPK pathway. J Exp Clin Cancer Res. 2016;35:148.
54. Ma B, Ueda H, Okamoto K, Bando M, Fujimoto S, Okada Y, et al. TIMP1 promotes cell proliferation and invasion capability of right-sided colon cancers via the FAK/Akt signaling pathway. Cancer Sci. 2022;113:4244–57.
55. Zheng S, Liang J-Y, Tang Y, Xie J, Zou Y, Yang A, et al. Dissecting the role of cancer-associated fibroblast-derived Biglycan as a potential therapeutic target in immunotherapy resistance: A tumor bulk and single-cell transcriptomic study. Clin Transl Med. 2023;13:e1189.
56. Zheng S, Zou Y, Tang Y, Yang A, Liang J-Y, Wu L, et al. Landscape of cancer-associated fibroblasts identifies the secreted Biglycan as a protumor and immunosuppressive factor in triple-negative breast cancer. Oncoimmunology. 2022;11:2020984.
57. Pan C, He Y, Wang H, Yu Y, Li L, Huang L, et al. Identifying patients with rapid progression from Hormone-Sensitive to Castration-Resistant prostate cancer: A retrospective study. Mol Cell Proteom. 2023;22:100613.
58. Melchionna R, Trono P, Di Carlo A, Di Modugno F, Nisticò P. Transcription factors in fibroblast plasticity and CAF heterogeneity. J Exp Clin Cancer Res. 2023;42:347.
59. Juang Y-L, Jeng Y-M, Chen C-L, Lien H-C. PRRX2 as a novel TGF-β-induced factor enhances invasion and migration in mammary epithelial cell and correlates with poor prognosis in breast cancer. Mol Carcinog. 2016;55:2247–59.
60. Rodríguez Y, Unno K, Truica MI, Chalmers ZR, Yoo YA, Vatapalli R, et al. A Genome-Wide CRISPR activation screen identifies PRRX2 as a regulator of enzalutamide resistance in prostate Cancer. Cancer Res. 2022;82:2110–23.
61. Wang J, Zhang Y, Chen X, Sheng Q, Yang J, Zhu Y, et al. Single-Cell transcriptomics reveals cellular heterogeneity and drivers in serrated Pathway-Driven colorectal Cancer progression. Int J Mol Sci. 2024;25:10944.
62. Mao Y, Schwarzbauer JE. Fibronectin fibrillogenesis, a cell-mediated matrix assembly process. Matrix Biol. 2005;24:389–99.
63. Cai X, Liu C, Zhang T-N, Zhu Y-W, Dong X, Xue P. Down-regulation of FN1 inhibits colorectal carcinogenesis by suppressing proliferation, migration, and invasion. J Cell Biochem. 2018;119:4717–28.
64. Erdogan B, Ao M, White LM, Means AL, Brewer BM, Yang L, et al. Cancer-associated fibroblasts promote directional cancer cell migration by aligning fibronectin. J Cell Biol. 2017;216:3799–816.
65. Ashok G, Ramaiah S. FN1 and cancer-associated fibroblasts markers influence immune microenvironment in clear cell renal cell carcinoma. J Gene Med. 2023;25:e3556.
66. Zhang X-X, Luo J-H, Wu L-Q. FN1 overexpression is correlated with unfavorable prognosis and immune infiltrates in breast cancer. Front Genet. 2022;13:913659.
67. Dzobo K, Sinkala M. Cancer stem cell marker CD44 plays multiple key roles in human cancers: immune suppression/evasion, drug resistance, Epithelial-Mesenchymal transition, and metastasis. OMICS. 2021;25:313–32.
68. Liu S, Liu Z, Shang A, Xun J, Lv Z, Zhou S, et al. CD44 is a potential immunotherapeutic target and affects macrophage infiltration leading to poor prognosis. Sci Rep. 2023;13:9657.
69. Kong T, Ahn R, Yang K, Zhu X, Fu Z, Morin G, et al. CD44 promotes PD-L1 expression and its Tumor-Intrinsic function in breast and lung cancers. Cancer Res. 2020;80:444–57.

70. Mao X, Xu J, Wang W, Liang C, Hua J, Liu J, et al. Crosstalk between cancer-associated fibroblasts and immune cells in the tumor microenvironment: new findings and future perspectives. Mol Cancer. 2021;20:131.
71. Huang T-X, Tan X-Y, Huang H-S, Li Y-T, Liu B-L, Liu K-S, et al. Targeting cancer-associated fibroblast-secreted WNT2 restores dendritic cell-mediated antitumour immunity. Gut. 2022;71:333–44.
72. Jenkins L, Jungwirth U, Avgustinova A, Iravani M, Mills A, Haider S, et al. Cancer-Associated fibroblasts suppress CD8 + T-cell infiltration and confer resistance to Immune-Checkpoint Blockade. Cancer Res. 2022;82:2904–17.
73. Tauriello DVF, Sancho E, Batlle E. Overcoming TGFβ-mediated immune evasion in cancer. Nat Rev Cancer. 2022;22:25–44.
74. Li T, Wang X, Niu M, Wang M, Zhou J, Wu K, et al. Bispecific antibody targeting TGF-β and PD-L1 for synergistic cancer immunotherapy. Front Immunol. 2023;14:1196970.
75. Tauriello DVF, Palomo-Ponce S, Stork D, Berenguer-Llergo A, Badia-Ramentol J, Iglesias M, et al. TGFβ drives immune evasion in genetically reconstituted colon cancer metastasis. Nature. 2018;554:538–43.
76. Mariathasan S, Turley SJ, Nickles D, Castiglioni A, Yuen K, Wang Y, et al. TGFβ attenuates tumour response to PD-L1 Blockade by contributing to exclusion of T cells. Nature. 2018;554:544–8.
77. Yi M, Wu Y, Niu M, Zhu S, Zhang J, Yan Y, et al. Anti-TGF-β/PD-L1 bispecific antibody promotes T cell infiltration and exhibits enhanced antitumor activity in triple-negative breast cancer. J Immunother Cancer. 2022;10:e005543.
78. Wong JKM, McCulloch TR, Alim L, Omer N, Mehdi AM, Tuong ZK, et al. TGF-β signalling limits effector function capacity of NK cell anti-tumour immunity in human bladder cancer. EBioMedicine. 2024;104:105176.

Publisher's note